Hierarchical SAPO-34 catalytic support for superior selectivity toward propylene in propane dehydrogenation process

Milad Komasi, Shohreh Fatemi[†], and Marjan Razavian

School of Chemical Engineering, College of Engineering, University of Tehran, P. O. Box 11365 4563, Iran

Abstract−SAPO-34 molecular sieve with tuned hierarchical structure was synthesized and used as the catalytic support for propane dehydrogenation (PDH) reaction to receive propylene with high selectivity. Synthesized material was characterized by XRD, FESEM, BET, ICP, FT-IR and TPO techniques. The Pt-Sn/SAPO-34 (hierarchical and regular ones) catalysts were prepared by impregnation method, and then the catalytic activity and selectivity of the catalysts were evaluated in PDH reaction. The results were compared with commercial Pt-Sn/γ-Al$_2$O$_3$ catalyst at the same operational conditions. Results revealed that hierarchical SAPO-34 based catalyst was the most efficient catalyst with superior activity and high propylene selectivity. The results suggested higher stability of the catalyst with hierarchical structure during seven hours reaction. Moreover, the impact of operational conditions was investigated on the performance of Pt-Sn/hierarchical SAPO for the temperature range of 550-650 $^\circ$C, weight hourly space velocity of 4 and 8 h^{-1} and H$_2$/C$_3$ molar ratios of 0.2-0.8, at normal pressure.

Keywords: Hierarchical SAPO-34, Pt-Sn/SAPO-34 Catalyst, Propane Dehydrogenation, Propylene

INTRODUCTION

Light olefins, such as ethylene, propylene, and butylene, are major basic chemical materials. Development of the global economy and rising availability of natural gas has caused continued interest in new roads to main petrochemicals such as propylene [1-3]. The demand for propylene has increased more quickly than for ethylene and butylene due to its increased application area in the production of polypropylene, acrylonitrile and other propylene downstream products [4]. There are two main means for propylene production: as a byproduct in thermal cracking of naphtha and from off-gases in fluid catalytic cracking (FCC) process. In these processes, yield of propylene is restricted by the demand for ethylene and gasoline, respectively. Therefore, development of on-purpose propylene production technologies is of the considerable interest.

Among the on-purpose propylene technologies, propane dehydrogenation (PDH) is relatively economical and the shortest route to propylene. Dehydrogenation is a viable option for increasing the supply of propylene in areas such as the Middle East with nearly cheap paraffin feedstock available [5-7]. The major process conditions are determined by thermodynamic limitations, reaction kinetics, and economics of the conversion-selectivity relationship [8]. Dehydrogenation of light paraffins comprises several technologies: Oleflex (UOP), STAR (Phillips Petroleum), Catofin (Houndry, United Catalysts Inc., ABB Lummus Crest), Linde-BASF, and FBD (Snamprogetti-Yarsintez). Employed catalysts are either promoted by Pt species being supported on various carriers (alumina and Group II spinels are preferred) or variously doped chromia-aluminas [9,10].

Chromia-alumina catalyst in dehydrogenation technology has been in use for many years. However, platinum-based catalysts have recently been preferred in alkane dehydrogenation because of the poisonous nature of chromium species. In the 1960s, Bloch [11] developed Pt-based catalysts that could selectively dehydrogenate long-chain linear paraffins to the corresponding internal mono-olefins with high activity and stability with minimum cracking side reactions [12]. Pt-Sn-based catalysts supported on Al$_2$O$_3$, SiO$_2$, and zeolites (ZSM-5, SAPO-34, etc.) have been discussed in many studies, and promising results have been reported [9, 13]. Recently, application of zeolites as catalyst has been extensively investigated in several petrochemical processes, experimentally and theoretically [14-16]. Pt-Sn/SAPO-34 as a highly selective catalyst gives a new technological trend in light olefin production via the direct dehydrogenation route. SAPO-34 is a micro-pore silicoaluminophosphate molecular sieve with chabazite structure containing eight-membered ring windows with mean pore diameter of 3.8 A$^\circ$. Relatively weak surface acidity (because most of the acid sites exist inside the pores) and large surface area of SAPO-34 provide superior dehydrogenation rate [4,17-19].

However, with an increasing need for fast diffusion of reactants and high conversion rates of bulky molecules, it is generally acknowledged that the intracrystalline diffusion limitations, stemming from the relatively small micropores, restrict the performance of industrial zeolitic catalysts. Diffusion limitations not only lead to a negative influence on catalytic activity, but also can cause a loss in selectivity and a reduction in the lifetime of the catalyst. Recently, the concept of introducing supplementary pores (meso-/macropores) into the zeolite materials and fabrication of hierarchically structured zeolites has gained increasing interest due to the combination of the advantages of both multimodal porous structure and zeolitic crystals. The introduction of two or three levels of porosities offers

an effective solution to achieve a faster migration of guest molecules in the host zeolite framework. Hierarchically structured zeolites possess superior catalytic activity compared to conventional zeolites, since they couple both the catalytic features of zeolitic micropores with improved accessibility and matter transport as a result of the additional larger pores all within a single system. Many catalytic tests confirm that hierarchically porous zeolites are much more catalytically active than conventional zeolites [20-23]. Today, a multitude of strategies have been employed to target the optimal design and synthesis of these materials. Soft templates were employed through double templating strategies to fabricate hierarchical SAPO-34 catalysts [24-26].

In this contribution, SAPO-34 molecular sieve with hierarchical tuned nanostructure was synthesized through a facile one-step hydrothermal route using a combination of amine agents [i.e., tetraethyl ammonium hydroxide (TEAOH), diethyl amine (DEA)] and polyethylene glycol (PEG), as structure directing and mesogenerating agents, respectively. Our aim was focused on the induction of tuned transport pores in the meso scale to advance the molecular diffusion property and enhance the accessibility of active sites within the cages and reduce the intervention of small micropores in the diffusion of reactants and products. This method is inexpensive and easily reproduced for high-yield production of SAPO-34 catalysts with excellent crystallinity. We further investigated the catalytic performance of the synthesized hierarchical SAPO-34-based sample in propane dehydrogenation reaction, aiming to reveal the intrinsic correlation between the catalytic effect and the accessibility of active sites, as well as the correlation between the accessibility and textural properties. Overall, we discuss here the performance of two types of Pt-Sn-based SAPO-34 with hierarchical and regular structure, respectively, and compare the results with a commercial catalyst to attain a broad picture for better understanding of the role of support in propane dehydrogenation. Moreover, the performance of Pt-Sn-based hierarchical SAPO-34 integrated catalyst was examined in a series of comparative tests to optimize the operational condition to boost the propylene yield.

EXPERIMENTAL

1. Synthesis of Catalysts

SAPO-34 molecular sieve was synthesized from a reaction mixture with molar composition of 1 Al_2O_3: 0.5 SiO_2: 0.65 P_2O_5: 0.1 HCl: 1.8 DEA: 0.2 TEAOH: 0.05PEG: 60 H_2O. First, aluminum isopropoxide (98%, Merck) was dissolved in mixed acid solution under vigorous stirring. Then tetraethyl orthosilicate (98%, Merck) was dissolved in basic template solution smoothly and was further added to aluminum solution. As the next step, polyethylene glycol (MW=4000, Merck) was added and the resultant gel was allowed to age and hydrolyze at room temperature for 24 h. Finally, the precursor gel was poured into Teflon lined stainless steel autoclave and was subjected to hydrothermal treatment in two steps of 130 $^{\circ}$C and 200 $^{\circ}$C for 17 h, respectively. The solid product was recovered and washed four times by centrifugation, and then dried at 120 $^{\circ}$C. Calcination was performed at 550 $^{\circ}$C for 5 h to remove the organic components.

For comparison, regular SAPO-34 particles were synthesized

through the same procedure without using PEG. These samples are named as SAPO-34 (without PEG) and H-SAPO-34 (with PEG).

2. Impregnation

Pt-Sn-based catalysts were prepared by a sequential impregnation method. First, the zeolite powder was impregnated in a 0.03 molar aqueous solution of $SnCl_2$. Second, the sample was impregnated in a 0.016 molar $PtCl_4$ aqueous solution, followed by drying at 80 $^{\circ}$C and calcining at 500 $^{\circ}$C for 6 h.

3. Catalyst Characterization Analysis

3-1. X-ray Diffraction (XRD) Analysis

The X-ray diffraction (XRD) patterns of powdered catalysts were obtained on a powder X-ray diffractometer (PHILIPS-binary) with a copper anode tube. The X-ray tube was operated at 40 kV and 30 mA. The spectra were scanned at a rate of 5 $^{\circ}$C/min, from 5 $^{\circ}$C to 50 $^{\circ}$C (an angular range 2θ).

3-2. FESEM

The morphology and particle size of the catalysts was studied by means of a field emission scanning electron microscope (ZEISS SIGMA VP) instrument.

3-3. BET Surface Area Measurement

The Brunner-Emmett-Teller surface area was measured by using N2 adsorption/desorption isotherms determined at liquid nitrogen temperature on an automatic multipoint BET analyzer (TriStar II 3020 V1.03 (V1.03)). The samples were outgassed for 1 h under vacuum at 300 $^{\circ}$C prior to adsorption. The specific BET surface areas of prepared samples were calculated by analyzing nitrogen adsorption data at 77 K in a relative vapor pressure ranging from 0.05 to 0.3. Micropore area and micropore volume were determined by t-plot method, and mean pore width (D_{avg}) was determined by BJH method.

3-4. Metallic Content Measurement

The metallic content was obtained by inductively coupled plasma atomic emission spectroscopy (ICP) measurement on a Varian ICP-OES Vista-pro spectrometer.

3-5. FT-IR

Chemical analysis was performed by Fourier transform infrared spectroscopy (FT-IR spectra) with a PerkinElmer spectrophotometer.

3-6. Temperature-programmed Oxidation for Coke Analysis

Temperature-programmed oxidation (TPO) of the catalyst was carried out after reaction for 7 h to analyze the type and location of the coke. 50 mg of reacted sample was used in each experiment. The samples were purged in argon at the flow rate 20 mL/min at 350 $^{\circ}$C for 1 h. Later the temperature was slowly decreased to 25 $^{\circ}$C. Then the mixture of 5% oxygen in helium by volume was passed through the samples at the flow rate of 20 mL/min. The temperature was ramped up at the rate of 10 $^{\circ}$C/min and the CO_2 was measured by an online gas analyzer TPx V1.03 (ChemiSoft).

4. Reaction Tests

Propane dehydrogenation was in a packed tubular quartz reactor inside an electrical furnace. A scheme of the experimental setup is shown in Fig. 1. The reactor was 1.2 cm in diameter and 50 cm long. The temperature was measured by three thermocouples at above, bottom, and the center of the catalyst bed, and the temperature was controlled by three PID controllers (JOMO) with ±1 $^{\circ}$C. The catalyst was inserted at the center of the bed and inert glass
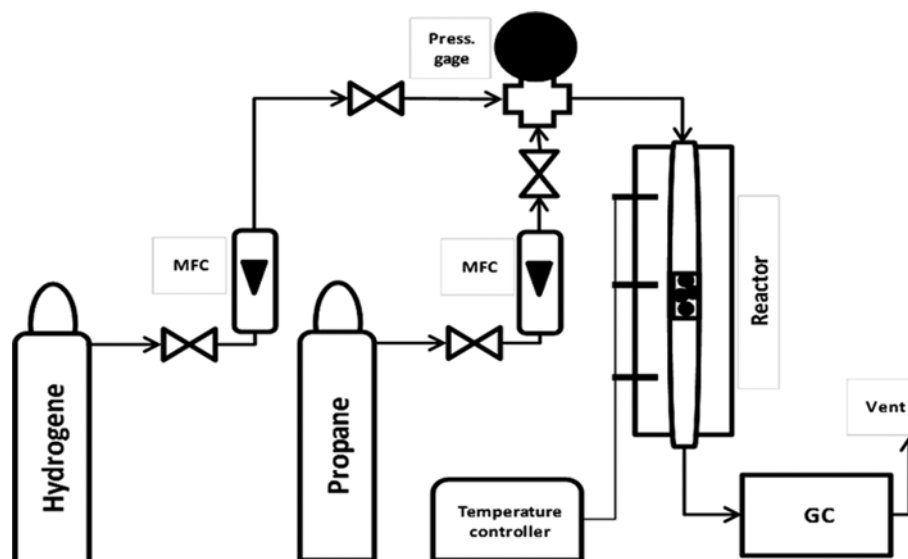
Fig. 1. Systematic PFD of reaction setup including feed capsules, MFCs, reaction zone and GC analyzer.

beads were used at the above and bottom of the catalyst. Three PID controllers maintained temperature variations of the setpoint. The zeolite powders were used without a binder and with mesh size of 30-60. The pretreatment of the catalyst was by flowing hydrogen stream at 500 °C for 2 h. Reaction took place at three different temperatures in the range of 550 to 650 °C, ambient pressure, and two different weight hourly space velocities (WHSV) of the feed of 4 and 8 h^{-1}. All the inlet flow rates were controlled by mass flow controllers (Brooks, 5850TR series). The reaction mixture was composed of H$_2$ and C$_3$H$_8$ with three different H$_2$/C$_3$H$_8$ molar ratios in the range of 0.2 to 0.8. The reaction products were analyzed with an online GC (gas chromatography YL6100) equipped with HID detector. Propane conversions and product selectivities were defined on the base of carbon content as follows [27]:

$$\text{Propane conversion (\%)} = \frac{\Sigma_i n_i F_{i,\,Out} - 3F_{C_3H_8,\,Out}}{\Sigma_i n_i F_{i,\,Out}} \times 100$$

$$\text{Selectivity comp. i (\%)} = \frac{n_i F_{i,\,Out}}{\Sigma_i n_i F_{i,\,Out} - 3F_{C_3H_8,\,Out}} \times 100$$

where i includes all the components with carbon atoms in the exit gas stream, n_i is the number of carbon atoms of component i, and F_i is its molar flow.

RESULTS AND DISCUSSION

1. Characterization

X-ray diffraction (XRD) patterns of synthesized samples are shown in Fig. 2. It is clear that the original structure/topology of the two SAPO-34 zeolite supports is the same. All major peaks are consistent with SAPO-34 standard reflections [28]. However, all the peaks in H-SAPO-34 sample are smoothed compared to SAPO-34 sample implying the existence of smaller crystals.

FESEM images are represented in Fig. 3. The SAPO-34 samples show polyhedron particles with a broad crystal size distribution, which range from 6-8 μm for regular SAPO (Fig. 3(a)) while
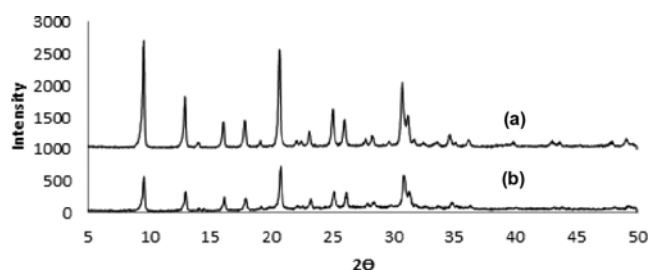

Fig. 2. Powder XRD patterns of (a) SAPO-34 and (b) H-SAPO-34 samples.

more uniform smaller cubic particles of about 3-4 μm were formed in H-SAPO-34 sample (Fig. 3(b)). The image of single particles is presented at the bottom of each figure to show any difference between the morphology of the formed particles. Intersectional topology of SAPO-34 particles confirms the presence of inert-crystalline diffusion paths resulting from close packing of primary crystallites, while long chains of wandering PEG polymer repelled H-SAPO-34 crystals from contacting one another and conglomeration. Therefore, it can be concluded that H-SAPO-34 crystals were less prone to aggregation during synthesis procedure because PEG molecules interacted with active sites of precursor and/or adsorbed onto the surface of the nuclei suppressing crystals adhesion. In addition, water soluble PEG polymer acted as swelling agent and shortened the nucleation period due to its water content reduction effect; therefore, more uniform and small crystals were obtained. Cubic shape of H-SAPO single particles quite contrary to the topology of SAPO-34 particles indicates the presence of diffusional pathways which are accessible from the outside of particles.

The textural and structural parameters obtained through nitrogen adsorption-desorption measurements for various samples are shown in Table 1. Surface area and pore volume of H-SAPO-34 are smaller than SAPO-34 sample with regular chabazite structure, which is consistent with those reported before [24,26,29].
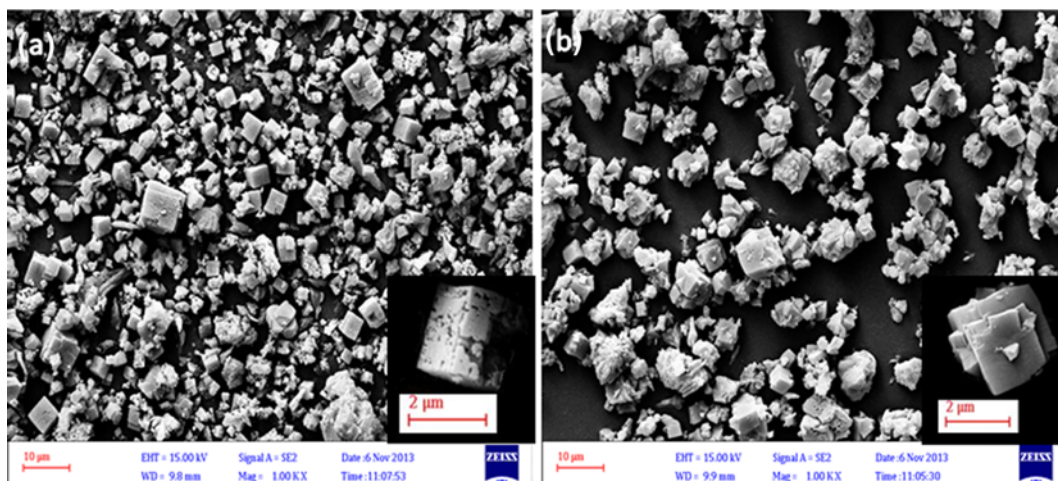
Fig. 3. SEM micrographs of (a) H-SAPO-34 and (b) SAPO-34.

Table 1. Results obtained from: (a) BET, (b) t-plot analysis and (c) BJH analyses

Sample	BET surface $(m^2/g)^a$	Micropore volume $(cm^3/g)^b$	Micropore area $(cm^2/g)^b$	Total pore volume (cm^3/g)	D_{avg} $(nm)^c$
SAPO-34	572.51	0.256	544.22	0.37	13.8
H-SPO-34	427.38	0.18	390.04	0.29	9.3
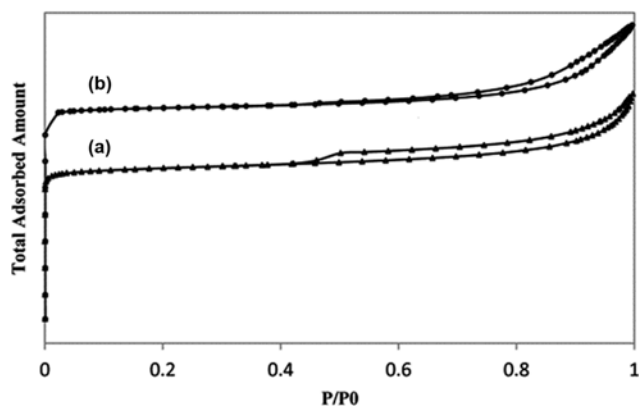
Fig. 4. The N2 adsorption-desorption isotherms of (a) H-SAPO-34 ($\triangle$), and (b) SAPO-34 ($\bigcirc$) samples.

Fig. 5. The BJH pore size distribution of (a) H-SAPO-34 ($\triangle$), and (b) SAPO-34 ($\diamondsuit$) samples.

Nitrogen adsorption-desorption isotherms of both samples are represented in Fig. 4. All isotherms are from the type of IV, which corresponds to mesoporous compound according to IUPAC classification [30]. The steep uptake in initial region ($p/p_0<0.1$) is a typical property of microporous materials. Hysteresis appearing in the physisorption isotherms is usually associated with capillary condensation taking place in mesopores. In fact, hysteresis loop shape is an identification of specific pore structure. Hysteresis loop shape in H-SAPO-34 samples is close to H4 type, which verifies the existence of narrow slit-like pores within material matrix, while H3 type shape in non-modified samples depicts the existence of slit-shaped pores which are the voids constructed upon aggregation of individual crystals. Intersectional topology of SAPO-34 particles in Fig. 3(b) confirms the presence of inert-crystalline diffusion paths resulting from close packing of primary crystallites, while long chains
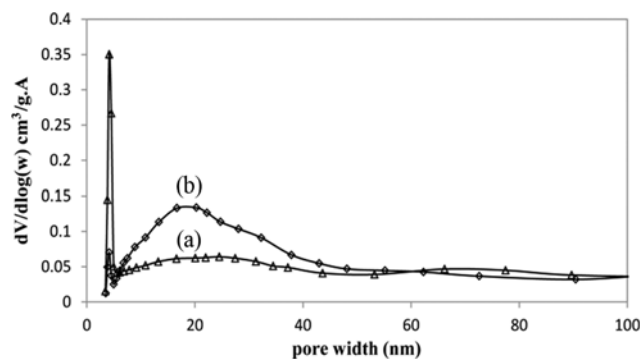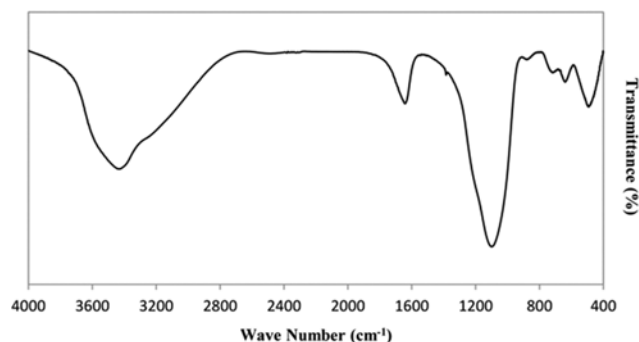
of wandering PEG polymer repelled H-SAPO-34 crystals from contacting one another and conglomeration.

Fig. 5(a) and (b) provides pore size distribution of both H-SAPO-34 and SAPO-34 samples. It can be concluded that PEG co-template tailored the porosity of H-SAPO-34 sample towards a tuned structure with a relatively large number of mesopores with a mean diameter of about 9 nm. The wide arc in SAPO-34 BJH pore size distribution curve is assigned to inter-crystalline mesopores that resulted from the close stacking of primary crystallites.

According to the literature, nominal metal composition of the samples was selected at 0.5 wt% Pt and 1.0 wt% Sn [31,32]. Selection of Sn as a promoter has been explained in terms of geometric and/or electronic effects. In the geometric effect, Sn decreases the size of platinum ensembles and reduces the rate of hydrogenolysis and coking reactions. Sn also modifies the electronic density of Pt, either by positive charge transfer from the Sn^{n+} species in Pt-Sn alloys [13,33]. The presence of Sn facilitates the transfer of coke

Table 2. Results from ICP analysis

Sample	Pt %wt	Sn %wt
Pt-Sn/HS	0.474	1.165
Pt-Sn/S	0.58	1.07

Fig. 6. FT-IR spectrum of H-SAPO-34 sample.

Table 3. Commercial catalyst characterization

Catalyst specifications		Major components (wt%)	
Shape	Sphere	Pt	0.6
Diameter (mm)	1.8	Sn	0.8
Specific surface (m^2/g)	200	K	0.8
Specific volume (g/cm^3)	0.65	Cl	1.36

Table 4. Deactivation parameter of the SAPO-34 catalysts

Sample	X_o	X_f	$D^* = ((X_0-X_f)/X_0)^*100$
Pt-Sn/H-SAPO-34	48.60	43.35	10.8
Pt-Sn/SAPO-34	42.70	36.63	14.21

from metal to support and the Pt dispersion, therefore significantly improving catalytic performance [18]. The metallic content was confirmed after successful impregnation of Pt and Sn on support, by using ICP analysis (see Table 2).

Fig. 6 demonstrates the FT-IR spectrum of H-SAPO-34 sample in a frequency range of 400-4,000 cm^{-1}. There is a broad band at 1,098 cm^{-1} assigned to the asymmetric stretching vibration of O-P-O groups. The absorption bands at 490, 640 and 730 cm^{-1} are typical characteristic bands of silicoaluminophosphate framework and attributed to the T-O bending of SiO_4 groups and double six-membered ring (D6R) subunits and symmetric stretching of P-O(Al-O) groups. A pronounced shoulder appears around 3,435 cm^{-1} in the spectrum which is ascribed to the stretching vibration of hydroxyl Si-OH-Al groups as strong acidic centers which are responsible active sites in acid-catalyzed reactions.

2. Catalyst Performance Analysis

The performance of the synthesized catalysts with two types of supports, regular SAPO-34 and hierarchical SAPO-34, in propane dehydrogenation reaction was compared with commercial Pt-Sn/ γ-Al_2O_3, and the results are shown in terms of conversion and pro-

pylene selectivity, in Fig. 7. The commercial Pt-Sn/γ-Al_2O_3 catalyst was supplied by Procatalyse Company (France) with the typical characteristics reported in Table 3 [34]. As shown in Fig. 7(a), the Pt-Sn/H-SAPO-34 demonstrates initial conversions of propane near thermodynamic equilibrium limits, i.e., 48.6%, at specified operating conditions (T: 600 °C; WHSV: 4 h^{-1}, H_2/C_3 molar ratio: 0.8). The conversion rate decreased to 43.35% after 7 h time on stream because of catalyst deactivation. Deactivation parameter of the synthesized catalysts after 7 h on stream is exhibited in Table 4. Deactivation parameter was calculated from the following relationship: $D = ((X_0-X_f)/X_0)^*100$, where X_0 is the initial propane conversion (after 1 h time on stream) and X_f is the final propane conversion (after 7 h time on stream). It can be observed that the reaction stability could be improved by using hierarchical intensified structure.

As shown in Fig. 7(b), remarkable propylene selectivity (91.23%) has been seen for this novel catalyst, which was reduced only 2.1% due to the formation of side products. Fig. 8 presents the product selectivities versus time on stream in PDH reaction. The modified Pt-Sn/H-SAPO-34 has exhibited high propane conversion and selectivity towards propylene in comparison with regular Pt-Sn/SAPO-34 and Pt-Sn/γ-Al_2O_3. Since the commercial catalyst contains large pores, its propylene selectivity is lower than hierarchical SAPO-34. In addition, lower propane conversion was achieved due to its lower surface area (200 m^2/g), whereas both SAPO-34 supported catalysts have sufficient surface area. Pt-Sn/SAPO-34 exhibited lower con-
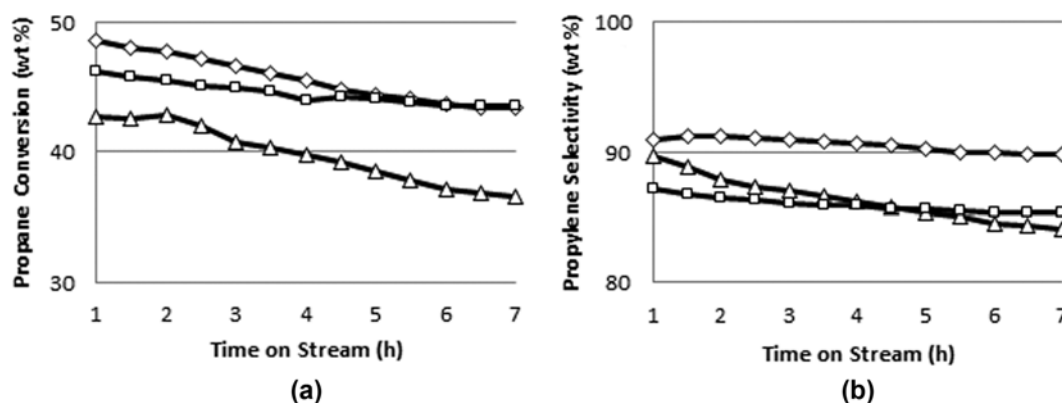

Fig. 7. (a) Propane conversion, and (b) propylene selectivity over: (◇) Pt-Sn/H-SAPO-34, (△) Pt-Sn/SAPO-34, and (□) Pt-Sn/γ-Al_2O_3 catalysts (T: 600 °C; WHSV: 4 h^{-1}, H_2/C_3 molar ratio: 0.8).
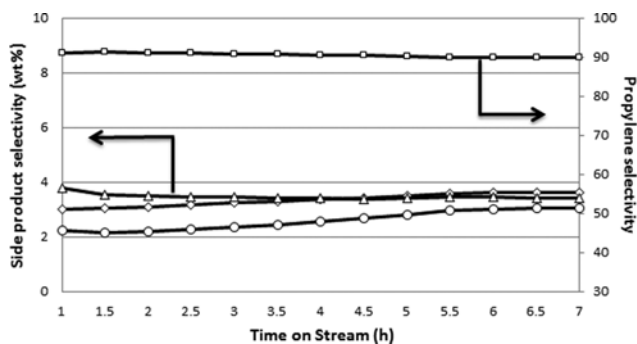
Fig. 8. Product selectivity on Pt-Sn/H-SAPO-34 (T: 600 °C; WHSV: 4 h⁻¹; H₂/C₃ molar ratio: 0.8): (□) propylene selectivity, (◇) methane, (○) ethylene, and (△) ethane selectivity.

Fig. 9. TPO profiles of different catalysts: (a) Pt-Sn/SAPO-34, and (b) Pt-Sn/H-SAPO-34.

version and selectivity towards propylene in comparison with Pt-Sn/H-SAPO-34, because of its narrower pore openings, whereas in modified SAPO-34 the mesopores have served as diffusion pathways [24] for reactants and products. In this case, molecules can diffuse without getting stuck in the pores and consequent blockage. As a result, more propane reached the active sites and was converted to olefin products.

3. TPO Analysis

Coke deposition on the catalyst is one of the most important side effects which directly influence the catalytic performance. Oxidation of the formed coke after 7 h catalytic reaction on different substrates was analyzed by temperature programmed oxidization (TPO) technique to obtain information on the location of carbon deposits. The results are shown in Fig. 9. The coked Pt-Sn-based catalysts showed a small peak located around 640 °C corresponding to the coke deposited on the external surface of the support and in zeolite channels, which is favorable for the reactants to access to the metallic active sites, thus improving the catalytic stability [31,35]. It is believed that the portion of coke occupying the support has little impact on the activity, and the activity can be easily resorted to after regeneration [14]. The Pt-Sn/SAPO-34 catalyst contains a higher amount of coke which is responsible for its higher catalyst deactivation. The coke deposited onto the catalyst can block the micropores of the support. The hierarchical SAPO-34 sample afforded better resistance to coking because of their interconnected
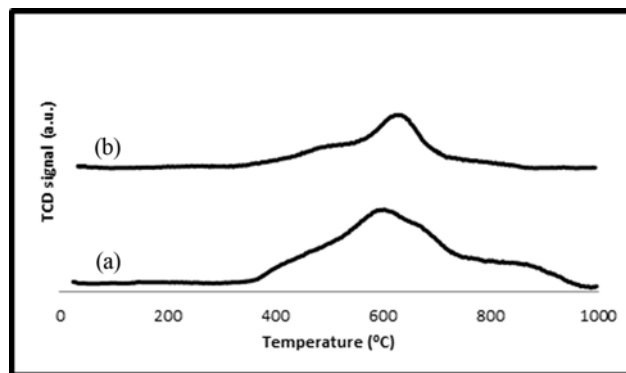
hierarchical porous structures. Similar results were observed in conversion of DME into olefins [24]. In Table 4, there is evidence for lower deactivation rate of hierarchical SAPO-34 catalyst against regular SAPO-34 one. Due to the existence of mesopores in hierarchical support, heavy carbonaceous compounds resulting from the side reactions of light olefin products that are literally counted as the primary precursors for the formation of coke, have deposited on the support, but a lower oxidation peak can be observed compared with that of regular SAPO, as seen in Fig. 9.

In addition, no peak in the range of 300-400 °C imiproves the efficiency of Sn loading procedure and successive transfer of carbon from metallic sites to the support. This phenomenon is only possible when there is good interaction between support and metals [36].

4. Influence of Operating Conditions

The synthesized catalysts have been tested under the same conditions (temperature of 600 °C, H₂/C₃ molar ratio of 0.8 and WHSV of 4 h⁻¹). The hierarchical SAPO-34 exhibited higher catalytic activity and stability than the conventional SAPO-34 in the conversion of propane to propylene; thus this catalyst was chosen for the subsequent tests.

According to Fig. 10, the reaction temperature is the most important factor which affects the performance of catalysts. This figure shows the effect of temperature on the performance of Pt-Sn/H-
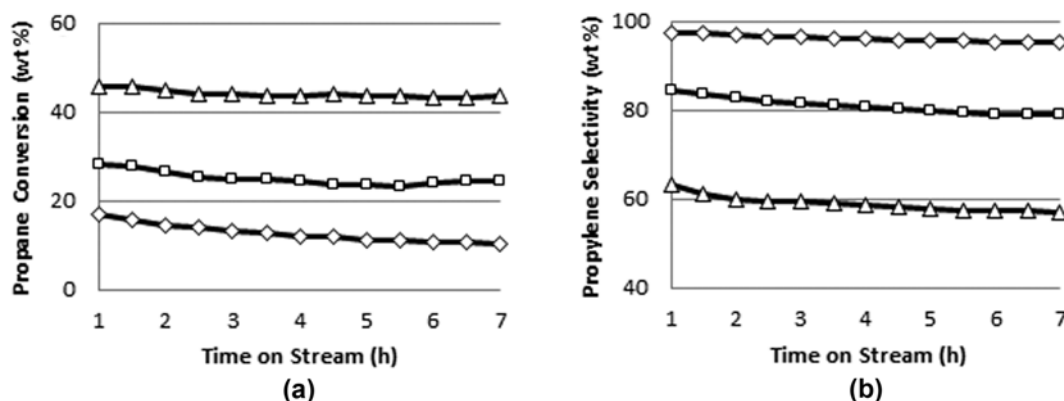

Fig. 10. Influence of temperature on (a) propane conversion, and (b) propylene selectivity at: (◇) 550 °C, (□) 600 °C, (△) 650 °C (H₂/C₃: 0.5; WHSV: 8 h⁻¹).
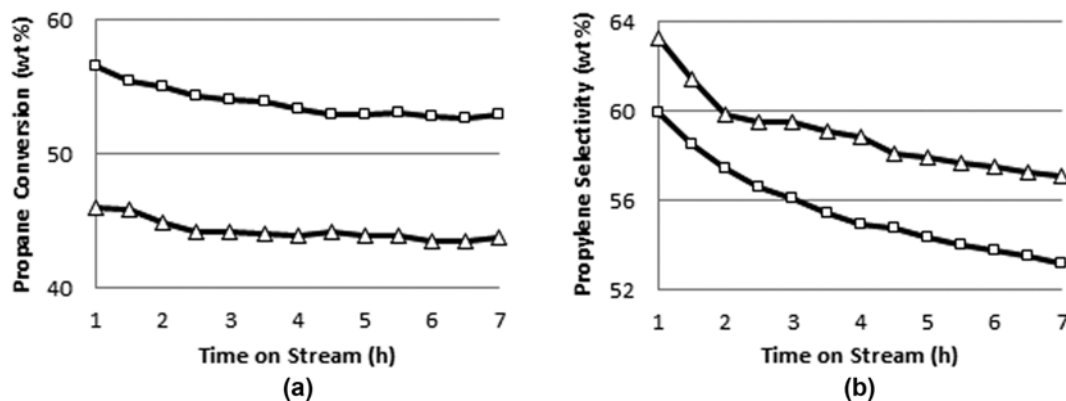
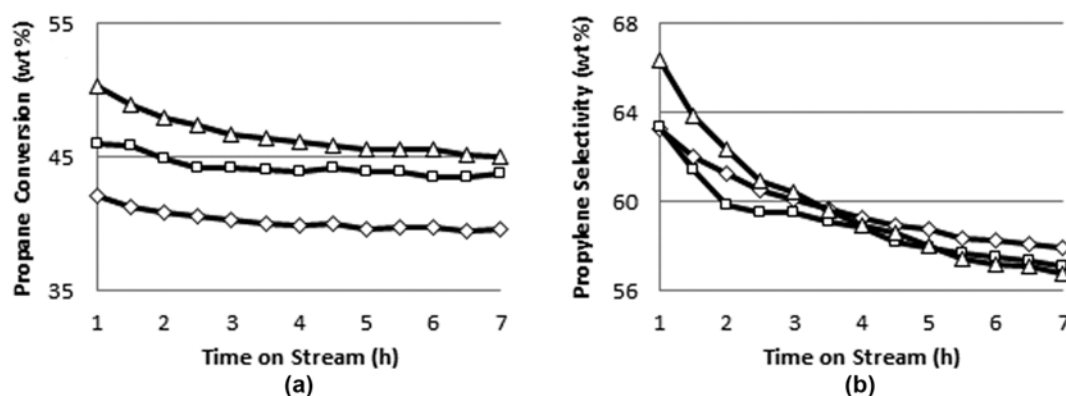**Fig. 11. Effect of WHSV on (a) propane conversion, and (b) propylene selectivity at: (□) 4 h⁻¹, (△) 8 h⁻¹ (H₂/C₃: 0.5; Reaction temperature: 650 °C).**

Fig. 12. Influence of H₂/C₃ molar ratio on (a) propane conversion, and (b) propylene selectivity at: (◇) 0.8, (□) 0.5, (△) 0.2 (reaction temperature: 650 °C; WHSV: 8 h⁻¹).

SAPO-34 catalyst in PDH reaction at a WHSV of 8 h⁻¹ and a H₂/C₃ molar ratio of 0.5. Dehydrogenation reaction is endothermic; therefore the propane conversion was improved with increasing reaction temperature. Meanwhile, a decrease of propylene selectivity was observed with an increasing reaction temperature. Obviously, this finding mainly resulted from the thermal/catalytic cracking of propane to the lighter hydrocarbons.

The influence of WHSV on the performance of selected catalyst is shown in Fig. 11 employed at two levels of 4 and 8 h⁻¹. Clearly, an increase in the WHSV could increase the propylene selectivity at the expense of lower conversion. The possible reason for this outcome might be related to the relatively short contact time at a high WHSV value, thus decreasing the amount of side reaction products.

The presence of H₂ can prevent the catalyst from rapid deactivation by reducing the coke formation [37]. Fig. 12 shows the effect of H₂/C₃ molar ratio on catalytic performance of Pt-Sn/H-SAPO-34 catalyst in PDH. Obviously, the propane conversion decreased significantly with increasing H₂/C₃ molar ratio; nevertheless, the selectivity to propylene remained almost unaffected. When the H₂/C₃ ratio was 0.2, the catalyst exhibited the highest activity.

CONCLUSIONS

A modified crystalline SAPO-34 molecular sieve with tuned hier-

archical structure was synthesized through a hydrothermal facile efficient procedure using PEG soft template. Catalytic performance of obtained material was evaluated in direct propane dehydrogenation reaction and compared with that of regular SAPO-34 and commercial γ-alumina. The PEG-modified SAPO-34 represented a superior activity for propane dehydrogenation to propylene (higher propylene selectivity and propane conversion) and less deactivation rate than regular SAPO-34. Due to the formation of less aggregated crystals with meso-intracrystalline pores as the result of PEG addition, active sites were successfully preserved from coke deposition and consequent deactivation. This great catalytic activity would be related to the suitable pore openings distribution in which reactants and products can diffuse more easily through the shorter diffusion pathways. The bigger space volumes inside the particles could increase the coke accommodation capacity of the pores with less effect on the active sites, thus preventing catalytic deactivation. The optimum reaction conditions have been also experimentally investigated over a range of operating parameters for the Pt-Sn/H-SAPO-34 catalyst.

NOMENCLATURE

PID : proportional integral derivative [-]
GC : gas chromatography [-]

HID   : helium ionization detector [-]
MFC : mass flow controller [-]
PDH : propane dehydrogenation [-]
WHSV: weight hourly space velocity [h^{-1}]
T   : temperature [^{o}C]
D_{ave} : mean pore width [nm]
i   : species [-]
n_i : number of carbon atoms of component i [-]
F_i : molar flow of species i [mol/min]
$F_{C_3H_8}$: molar flow of propane [mol/min]
D   : deactivation parameter [-]
X_0 : initial propane conversion [-]
X_f : final propane conversion [-]
θ : diffraction angle [degrees]

REFERENCES

1. X. Li, C.-H. Li, Q. Yuan, C.-H. Yang, H.-G. Shan and J. Zhang, *Am. Chem. Soc.*, **48**, 910 (2003).
2. AL WAHABI S-M, Texas A&M University (2003).
3. J.-Q. Chen, A. Bozzano, B. Glover, T. Fuglerud and S. Kvisle, *Catal. Today*, **106**, 103 (2005).
4. H. Zhou, Y. Wang, F. Wei, D.-Z. Wang and Z.-H. Wang, *Appl. Catal. A: General*, **348**, 135 (2008).
5. Z. Nawaz and F. Wei, *J. Ind. Eng. Chem.*, **17**, 389 (2011).
6. S. Airaksinen, *Chromium oxide catalysts in the dehydrogenation of alkanes*, Industrial Chemistry Publication Series, Finland (2005).
7. J.-A. Medrano, I. Julian, J. Herguido and M. Menendez, *Membranes*, **3**, 69 (2013).
8. H. A. Wittcoff, B. G. Reuben and J. S. Plotkin, *Industrial arganic chemicals*, John Wiley & Sons (2012).
9. M.-P. Lobera, C. Tellez, J. Herguido and M. Menendez, *Ind. Eng. Chem. Res.*, **47**, 9314 (2008).
10. M. Heinritz-Adrian, S. Wenzel and F. Youssef, *Petroleum Technology Quarterly*, **13**, 83 (2008).
11. H.-S. Bloch, Skokie, US Patent, 3,448,165 (1969).
12. M.-M. Bhasin, J.-H. McCain, B.-V. Vora, T. Imai and P.-R. Pujado, *Appl. Catal. A: Gen.*, **221**, 397 (2001).
13. Z. Nawaz, F. Baksh, J. Zhu and F. Wei, *J. Ind. Eng. Chem.*, **19**, 540 (2013).
14. Y. Zhang, Y. Zhuo, A. Qiu, Y. Wang, Y. Xu and P. Wu, *Ind. Eng. Chem. Res.*, **45**, 2213 (2006).
15. Z. Nawaz, Y. Chu, W. Yang, X. Tang, Y. Wang and F. Wei, *Ind. Eng. Chem. Res.*, **49**, 4614 (2010).
16. S. Askari, R. Halladj and M. Sohrabi, *Micropor. Mesopor. Mater.*, **163**, 334 (2012).
17. L. Zhang, J. Bates, D.-G. Chen, H.-Y. Nie and Y. Huang, *J. Phys. Chem. C*, **115**, 22309 (2011).
18. Z. Nawaz and F. Wei, *J. Ind. Eng. Chem.*, **16**, 774 (2010).
19. Z. Nawaz, X. Tang, Y. Chu and F. Wei, *Chinese J. Catal.*, **31**, 552 (2010).
20. G.-J.-d. Soler-Illia, C. Sanchez, B. Lebeau and J. Patarin, *Chem. Rev*, **102**, 4093 (2002).
21. Z. Xue, T. Zhang, J.-G. Ma, H. Miao, W. Fan, Y. Zhang and R. Li, *Micropor. Mesopor. Mater.*, **151**, 271 (2012).
22. C.-E.-A. Kirschhock, S.-P.-B. Kremer, J. Vermant, G. Van Tandeloo, P.-A. Jacob and J.-A. Martens, *Chemistry-a European Journal*, **11**, 4306 (2005).
23. L.-H. Chen, X.-Y. Li, J.-C. Rooke, Y.-H. Zhang, X.-Y. Yang, Y. Tang, F.-S. Xiao and B.-L. Su, *J. Mater. Chem.*, **22**, 17381 (2012).
24. Y. Cui, Q. Zhang, J. He, Y. Wang and F. Wei, *Particuology*, **11**, 468 (2013).
25. F. Schmidt, S. Paasch, E. Brunner and S. Kaskel, *Micropor. Mesopor. Mater.*, **164**, 214 (2012).
26. L. Kong, Z. Jiang, J. Zhao, J. Liu and B. Shen, *Catal. Lett.*, **144**, 1609 (2014).
27. M.-P. Lobera, C. Tellez, J. Herguido and M. Menendez, *Appl. Catal. A: Gen.*, **349**, 156 (2008).
28. M.-M. Treacy and J.-B. Higgins, Collection of Simulated XRD Powder Patterns for Zeolites Fifth (5th) Revised Ed., Elsevier (2007).
29. W. Guo, G.-S. Luo and Y.-J. Wang, *J. Colloid Interface Sci.*, **271**, 400 (2004).
30. K.-S. Sing, *Pure Appl. Chem.*, **57**, 603 (1985).
31. Z. Nawaz, X. Tang, Y. Wang and F. Wei, *Ind. Eng. Chem. Res.*, **49**, 1274 (2009).
32. Z. Nawaz, X. Tang and F. Wei, *Korean J. Chem. Eng.*, **26**, 1528 (2009).
33. Z. Nawaz, X. Tang, Q. Zhang, D. Wang and W. Fei, *Catal. Commun.*, **10**, 1925 (2009).
34. M. Fattahi, F. Khorasheh, S. Sahebdelfar, F. Tahriri Zangeneh, K. Ganji and M. Saeedzad, *Scientia Iranica*, **18**, 1377 (2009).
35. E. Epelde, M. Ibañez, A.-T. Aguayo, A.-G. Gayubo, J. Bilbao and P. Castaño, *Micropor. Mesopor. Mater.*, **195**, 284 (2014).
36. E. Brevoord, A.-C. Pouwels, F.-P.-P. Olthof, H.-N.-J. Wijngaards and P. O'Connor, *Am. Chem. Soc.*, **25**, 340 (1996).
37. M. van Sint Annaland, J.-A.-M. Kuipers and W.-P.-M. Van Swaaij, *Catal. Today*, **66**, 427 (2001).